

# Indoor Human Trajectory Reconstruction via Multi-link mmWave Passive Sensing System

Renqi Chen

**Abstract**—Indoor multi-target trajectory reconstruction based on passive sensing has been studied for decades. Most existing solutions stay in the sub-6 GHz band, which can only track single target while retaining considerable error. Although millimeter wave (mmWave) radar has shown potential for multi-target tracking, active sensing is not suitable for the application context of integrated sensing and communication (ISAC). This paper aims to overcome these limitations through a multi-link mmWave communication sensing system that can track multiple targets. Our design consists of three core components. Firstly, mmWave array antennas are employed to collect communication signals and extract multi-link Doppler frequency shift (DFS) by cross ambiguity function (CAF), while applying clustering and path-matching algorithms to do fine-grained processing. Secondly, further derivation of the DFS-velocity relationship is applied to obtain the correct correspondence. Thirdly, digital beamforming is implemented on the mmWave phased array using beam search methodology, followed by the multiple signal classification (MUSIC) to estimate the multi-link arrival of angles (AoAs) and initial position. Eventually combine the velocity with initial position to achieve trajectory reconstruction. We implement the system upon transmitting a 802.11a compliant multi-carrier signal. Experiments demonstrate that the proposed system achieves respective median errors of single target and two targets lower than 15 cm and 22 cm.

**Index Terms**—ISAC, mmWave, passive sensing, tracking, multi-target

## I. INTRODUCTION

Within the last few decades, as communication devices showed exponential growth, the sub-6 GHz band became confined and the millimeter wave (mmWave) band was focused [1]. Meanwhile, in the context of integrated sensing and communication (ISAC), people desired to realize communication while using passive sensing techniques (device-free for the sensed targets, no need for additional lighting sources and no connection between the transmitter and the receiver) to perform sensing tasks, including target localization, trajectory tracking, and gesture recognition, etc. For the trajectory tracking task of concern, due to complex micro-Doppler of the human body, tracking error would continue to superimpose as the trajectory time becomes longer. Therefore, mmWave was given high expectation because of the advantage of being more sensitive to Doppler than sub-6 GHz. Thus, a robust mmWave passive sensing system needs to reach the goal of achieving lower error and recognizing multiple targets.

In sub-6 GHz band, indoor trajectory tracking based on passive sensing techniques has been progressed in recent years

R. Chen is with the Department of Electronic and Electrical Engineering, Southern University of Science and Technology, China (email: 11910818@mail.sustech.edu.cn).

[2–5]. In [2], single-person trajectory tracking was facilitated through calculating Doppler frequency shift (DFS) from multiple links (one transmitter, multiple receivers) of channel state information (CSI). By manually adjusting the direction of target in long-distance trajectory tracking, it realized a median error of 35 cm. In addition to DFS, arrival of angle (AoA) is also taken into account [3, 4]. [3] implemented a median error of 60 cm by evaluating the multi-link AoA. As both AoA and DFS assist in tracking, multidimensional information was considered in [4]. A median error of 75 cm was achieved by obtaining the CSI of a single link to extract the DFS, combined with the AoA and time-of-flight (ToF). Recently, in [5], as the closed-form solution for Doppler-velocity relationship was derived, a median error of 31 cm was realized by multi-link DFS. Nevertheless, tracking error always maintained at a large value due to the low Doppler resolution of sub-6 GHz band limited by long wavelength of physical property, and all experimental scenarios were single target.

In fact, the research of trajectory tracking in mmWave band was advanced based on mmWave radar [6, 7], relevant to the task in passive sensing. In [6], target distance variation information was extracted by channel impulse response (CIR), and with the assistance of clustering technique, multi-target recognition and trajectory reconstruction were implemented with a respective 90% accuracy of 22.5 cm and 35.6 cm for static and dynamic scenarios, respectively. Deep learning methods were also adopted [7]. In [7], use deep learning network to train the CSI fingerprints, accuracy reached 54 cm in specific scenario. Although mmWave radar enabled to obtain low error results for multi-target trajectory tracking, this is not compatible with passive sensing and cannot be applied in the context of ISAC. Table I provides a comprehensive comparison of the tracking system based on passive sensing or active sensing.

Although there have been numbers of trials and experimental results of trajectory reconstruction task based on the passive sensing techniques in sub-6 GHz band, there is still no methodology in mmWave band, especially for multi-target scenarios. Thus, it is natural to extend to mmWave band, which would have higher Doppler resolution because of the smaller wavelength. In this paper, a multi-link mmWave passive sensing system for indoor human trajectory reconstruction is proposed. The 16-antenna mmWave phased arrays are deployed at both transmitter and receiver. Specifically, single-target scenario and multi-target scenarios are developed by velocity and initial position estimation, where velocity is estimated by multi-link DFS and initial position is estimated

TABLE I  
COMPARISON OF STATE-OF-THE-ART TRACKING SYSTEMS.

Category	System Name	Frequency Range	Single Target Error (Median Error)	Multiple Target Error (Median Error)	Parameter
Active	mmTrack[6] FreeTrack[7]	mmWave mmWave	9.9 cm 54 cm	19.7 cm -	CIR CSI Fingerprint
Passive	Widar[2] Widar2.0[4] Dynamic Music[3] PITrack[5] <b>Ours</b>	sub-6 GHz sub-6 GHz sub-6 GHz sub-6 GHz <b>mmWave</b>	35 cm 75 cm 60 cm 31.08 cm <b>&lt;15 cm</b>	- - - - <b>&lt;22 cm</b>	DFS DFS, AoA, ToF AoA DFS <b>DFS, AoA</b>

by multi-link AoA. Note that our system realizes that the respective median errors of 15 cm and 22 cm for single target and two targets.

The remainder of this paper is organized as follows. In Section II, an overview of the mmWave passive sensing system is introduced. The signal processing algorithm for passive sensing is introduced in Section III. In Section IV, the methodology for tracking is proposed. The experiment results and discussion are provided in Section V. Finally, the conclusion is drawn in Section VI.

## II. SYSTEM OVERVIEW

Indoor human trajectory reconstruction is implemented with an integrated passive sensing and communication system, as elaborated in Fig. 1, which consists of one transmitter and one receiver. Specifically, there are at least three radio frequency (RF) chains at the receiver, where each RF chain is corresponding to one phased array with N antenna elements. To ensure the simultaneous communication and sensing, three phased arrays share the clock signals.

As illustrated in Fig. 1, the side lobe of transmitter beam is directed towards one of the phased arrays called reference antenna, where the signal arrives at the receiver via the static propagation path without DFS called reference channel, represented by black dotted line. Meanwhile, the signals from main lobe firstly arrives at the target and then are reflected to the other two phased arrays called surveillance antennas through the paths referred as surveillance channels. The more considered beam ranges at the transmitter and receiver ends are depicted using purple and green dashed lines, respectively. Suppose the target is in the detection district, the signals received by the reference channel can be applied for communication, and the multi-link DFS can be obtained by comparing the signals received by the reference channel with those received by multiple surveillance channels, which enables the track reconstruction.

## III. SIGNAL PROCESSING OF PASSIVE SENSING

### A. Signal Model

Without loss of generality, the analysis is performed for the  $m^{th}$  moment of the target movement. Let the  $s_m(t)$  be the current transmitted signal. The signal received at the reference antenna can be written as

$$y_r(t) = \alpha_r s_m(t - \tau_r) + n_r(t), \quad (1)$$

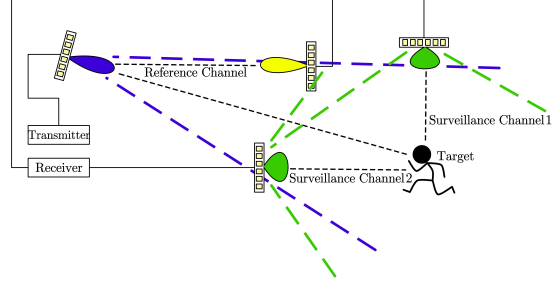


Fig. 1. System overview.

where  $t$  is the time,  $\alpha_r$  and  $\tau_r$  denote the complex gain and delay of the reference channel, respectively, and  $n_r(t)$  denotes the noise in the reference channel.

For signals received at the two surveillance antennas, consider the multi-path clutters, then we have

$$y_{s,i}(t) = \sum_{l=1}^M \alpha_{s,i}^l s_m(t - \tau_{s,i}^l) e^{-j2\pi f_{d,i}^l t} + n_{s,i}(t), \quad (2)$$

where  $M$  is the number of echo paths in the  $i^{th}$  surveillance channel,  $\alpha_{s,i}^l$ ,  $\tau_{s,i}^l$  and  $f_{d,i}^l$  denote the complex gain, delay and DFS of the  $l^{th}$  path in the  $i^{th}$  surveillance channel, respectively,  $n_{s,i}$  is the noise in the  $i^{th}$  surveillance channel.

### B. Doppler Estimation

After receiving and sampling the signals from reference channel and two surveillance channels, estimate the time-DFS spectrum by the following cross ambiguity function (CAF),

$$R(f_{d,i}, t) = \max_{\tau} \int_t^{t+T_w} y_{s,i}(x) y_r^*(x - \tau) e^{j2\pi f_{d,i} x} dx, \quad (3)$$

where  $(.)^*$  is the complex conjugate and  $T_w$  is length of correlation integration time (CIT). Noticed that the larger CIT, the higher Doppler resolution. However, it also brings higher computation complexity and mixture of DFS of varying time. Moreover, due to the direct path and static objects, there usually exists strong zero-DFS signal in time-DFS spectrum, which can be cancelled by the clutter cancellation [8].

## IV. TRACKING MODEL

In this section, tracking model is illustrated in Fig. 2, which is composed three main modules: DFS extraction, velocity derivation and track reconstruction. The flow chart can be

summarized as reference and surveillance signals are collected from mmWave array antennas and performed DFS extraction. Then output the available DFS to track reconstruction, where the initial position is estimated, combined with DFS-based computing velocity to determine the trajectory.

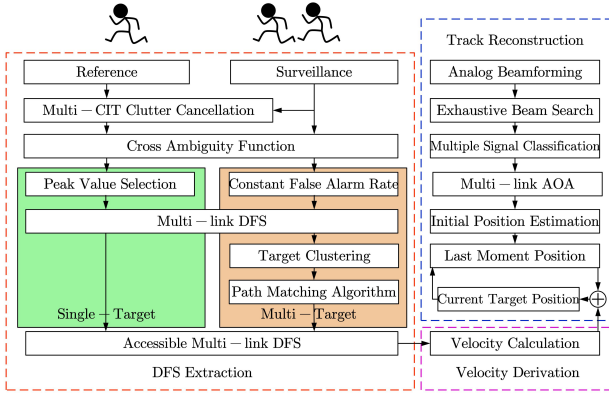


Fig. 2. Tracking model processing flow chart.

### A. DFS Extraction

In our system, coarse time-DFS spectrum  $R(f_{d,i}, t)$  are calculated by formula (3) after multi-CIT clutter cancellation which aims to reduce static interference while avoiding damage to motion integrity.

For single target scenario, at each CIT slot, we only focus on the DFS corresponding to the peak value of CAF, which is referred as causing by the target and is capable of describing the movement in a comprehensive way,

$$\hat{f}_{d,i}(t) = \arg \max_{f_{d,i}} R(f_{d,i}, t). \quad (4)$$

For multi-target scenario, peak value selection is no longer applicable as multiple targets possess different DFS intensities. The global picture cannot be taken into account when selecting the largest few peaks. Then we choose Constant False Alarm Rate (CFAR) [9] to determine the possible points, detection threshold is given by

$$\beta(f_{d,i}, t) = \frac{1}{2L+1} \sum_{g=-L}^L R(f_{d,i} + g \frac{1}{CIT}, t), \quad (5)$$

where  $L$  is the half length of training cells and  $\frac{1}{CIT}$  is the Doppler resolution.

The all possible DFS in each time slot are given by

$$\Gamma_i^t = \{f_{d,i} | R(f_{d,i}, t) \geq \beta(f_{d,i}, t)\}, \quad (6)$$

where  $\Gamma_i^t$  is a set includes all satisfied DFS at time  $t$ .

Next, design a target clustering algorithm to distinguish the DFS points belong to the respective movement of multiple targets. The key factor is to determine target number, solved in initial position estimation discussed in IV-C (when the initial position of targets are found, it is simple to count the number of them). And we choose DBSCAN clustering [10] as main body, which is possible to cluster data sets of arbitrary shape and discover outliers. Then, by refining clustering results with

target number estimated as category number of the former differs from the latter, DFS that belongs to respective targets is separated cleanly.

In order to select reasonable DFS trajectory from clustering results, a simple path matching algorithm is proposed. For each target, initial DFS point begins at the time slot that exists DFS, estimated as the mean value if there are multiple points meanwhile, marked as  $\Theta_{before}$ , then consider next time slot  $t_{current}$ .

a) *No DFS Exists at  $t_{current}$* : As CFAR allows no DFS points, when this case occurs, traverse future moments until a DFS-existing moment is discovered, and remark the mean value of DFS of this moment as  $\Theta_{after}$ . Define DFS of current time slot by linear interpolation as

$$\Theta_{current} = \Theta_{before} + \frac{\Theta_{after} - \Theta_{before}}{t_{after} - t_{before}} (t_{current} - t_{before}), \quad (7)$$

where  $t_{before}$  and  $t_{after}$  denote the time slot of  $\Theta_{before}$  and  $\Theta_{after}$ , respectively. Then, update  $\Theta_{after}$  equals to  $\Theta_{current}$ .

b) *DFS Exists at  $t_{current}$* : Another case is current slot exists one or more DFS points. Considering the continuity of motion and the tendency to more pronounced DFS,  $\Theta_{current}$  can be chosen as

$$\Theta_{current} = \arg \max_{f_d \in \Gamma_{i,p}^{t_{current}}} \varepsilon \cdot e^{-dist(f_d, \Theta_{before})} + \zeta \cdot |f_d| \quad (8)$$

where  $\Gamma_{i,p}^{t_{current}}$  denotes existing DFS points in the distinguished set for the  $p^{th}$  target in the  $i^{th}$  surveillance channel at  $t_{current}$ ,  $dist(\cdot)$  is the distance function,  $|\cdot|$  is the absolute value, and  $\varepsilon$  and  $\zeta$  are both weight coefficients. Then update in the same way as before.

By this algorithm, the path is continuously matched until the last time slot and accessible multi-link DFS are extracted.

### B. Velocity Derivation

After extracting DFS information, derive the relationship between the multi-link DFS and velocity of target.

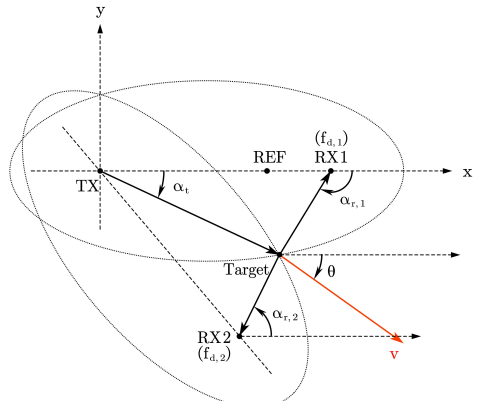


Fig. 3. Illustration of coordinate system.

A coordinate system is elaborated in Fig. 3, where RX1 and RX2 illustrate the first and the second surveillance antennas, TX illustrates the transmitter, and REF illustrate the reference

antenna. According to [5], the relationship between DFS and velocity can be given as follows,

$$\begin{cases} f_{d,1} = -\frac{f_o}{c} \cdot v \cos(\theta - \frac{\alpha_{r,1} + \alpha_t}{2}) \cdot 2 \cos(\frac{\alpha_{r,1} - \alpha_t}{2}), \\ f_{d,2} = -\frac{f_o}{c} \cdot v \cos(\theta - \frac{\alpha_{r,2} + \alpha_t}{2}) \cdot 2 \cos(\frac{\alpha_{r,2} - \alpha_t}{2}), \end{cases} \quad (9)$$

where  $f_{d,1}$  and  $f_{d,2}$  denote the DFS of two surveillance channels respectively,  $\alpha_t$  denotes the angle of departure,  $\alpha_{r,1}$  and  $\alpha_{r,2}$  denote the arrival of angles of RX1 and RX2 respectively,  $f_o$  is the frequency of transmitted signals,  $c$  is the speed of light,  $v$  and  $\theta$  denote the speed and direction of target velocity respectively.

Given the location of TX, RX1 and RX2, when the initial position of target is estimated,  $\alpha_t$ ,  $\alpha_{r,1}$  and  $\alpha_{r,2}$  can be measured and then solve (9) for velocity as follows,

$$\begin{bmatrix} v_x \\ v_y \end{bmatrix} = \mathbf{F}^{-1} \begin{bmatrix} f_{D1} \\ f_{D2} \end{bmatrix}, \quad (10)$$

where  $v_x = v \cos \theta$ , denoting the velocity component in the x-direction,  $v_y = v \sin \theta$ , denoting the velocity component in the y-direction, and  $\mathbf{F}$  is defined as

$$\mathbf{F} = -\frac{2f_o}{c} \cdot \left( \begin{bmatrix} \cos(\frac{\alpha_{r,1}-\alpha_t}{2}) \cos(\frac{\alpha_{r,1}+\alpha_t}{2}) & \cos(\frac{\alpha_{r,1}-\alpha_t}{2}) \sin(\frac{\alpha_{r,1}+\alpha_t}{2}) \\ \cos(\frac{\alpha_{r,2}-\alpha_t}{2}) \cos(\frac{\alpha_{r,2}+\alpha_t}{2}) & \cos(\frac{\alpha_{r,2}-\alpha_t}{2}) \sin(\frac{\alpha_{r,2}+\alpha_t}{2}) \end{bmatrix} \right). \quad (11)$$

### C. Track Reconstruction

In this module, initial position estimation is considered, always computed from AoAs by Multiple Signal Classification (MUSIC). Nevertheless, as normally mmWave phased array antenna uses analog beamforming, where receiver antenna uses combiner to merge received signal on each antenna unit, MUSIC cannot be applied. Hence we consider constructing digital beamforming by exhaustive beam search in [11], estimating signal by periodically transmitting the same signal  $N_T$  times at TX and receiving the signal using  $N_R$  different analog combiners, which can be implemented by turning on different numbers and positions of antenna units on the mmWave phased array at RX.

Noticed that when only AoA is focused, this estimation can be simplified as

$$\hat{s}(t) = \mathbf{E}\mathbf{y}(t), \quad (12)$$

where  $\mathbf{E} = [\mathbf{e}_1, \mathbf{e}_2, \dots, \mathbf{e}_{N_R}]$ , is a unitary matrix in actual scenario, composed of  $N_R$  different analog combiners weights,  $\mathbf{y}(t)$  is the received signal after combiners at the receiver, which is a  $N_R \times 1$  vector. Then signal arriving at  $q^{th}$  antenna unit and signal covariance matrix can be expressed as

$$m(t) = \mathbf{s}_q(t), \quad (13)$$

and

$$\Sigma = \mathbf{mm}^H. \quad (14)$$

Then MUSIC can be applied and multi-link AoA are solved, determining the target number for clustering and evaluating the initial position through the intersection region of AoAs.

Based on initial position and velocity obtained from IV-B, trajectory can be reconstructed. Specifically, as shown in Fig. 2, current target position is calculated by the last moment position (initial position is the first “last moment position”) and current moment velocity, and then it becomes the last moment position for the next moment position estimation. Meanwhile,  $\alpha_t$ ,  $\alpha_{r,1}$  and  $\alpha_{r,2}$  in formula (9) are updated. By iterating continuously, trajectory reconstruction is completed.

## V. EXPERIMENTS AND DISCUSSION

### A. Implementation

Based on software-define radio (SDR) and mmWave phased array, the mmWave communication and sensing system is constructed shown in Fig. 4. At transmitter portion, noticed that TX consists one NI USRP-2953R and one Sivers 60 GHz phased array antenna. Under the context of ISAC, transmitter host transmits the communication signal which is a multi-carrier signal compliant with 802.11a protocol with a 20 MHz bandwidth over the downlink. To further enhance the perception, the beam width of TX is 50° and directs at the detection area. At receiver portion, it consists of REF, RX1 and RX2. Three Sivers 60 GHz phased array antennas with synchronized clocks are connected to three channels of two USRPs. As no need time delay to determine the range information, the sampling rate of USRPs is set to 10 MHz. Note that RX2 outputs clock signal to RX1 and REF to synchronize to eliminate carrier offset. The beam width of REF is 10°, directing at TX, and the beam width of RX1 and RX2 are all 130°, directing at detection area and are perpendicular to each other. After a predefined detection duration, receiver host read the data collected by USRPs through Gigabit Ethernet port. In this paper, the length of CIT is chosen as 0.1 s.

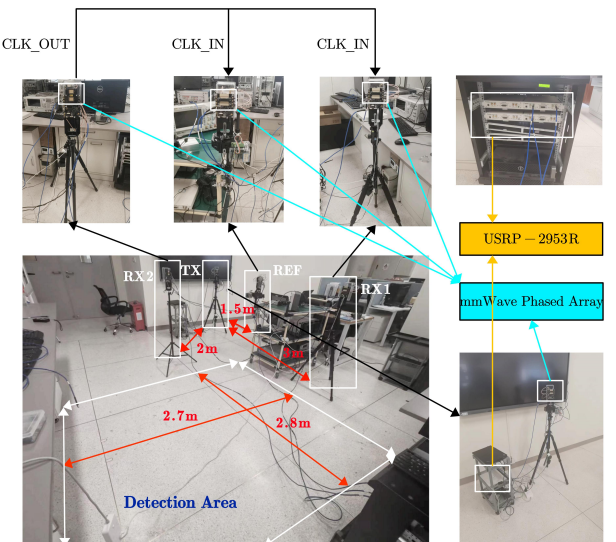


Fig. 4. Experimental scenario and device setup.

As elaborated in Fig. 4, our experimental scenario is an indoor environment. The distance between transmitter and REF, RX1 and RX2 are 1.5 m, 3 m, 2 m, respectively. The detection area can be approximated as a  $2.7 \text{ m} \times 2.8 \text{ m}$  rectangular district where the targets move. All of the phased arrays are placed at a height of 1.45 m.

### B. DFS and AoA Estimation

Fig. 5 presents two examples of single target and two targets experimental scenarios, and Fig. 6 illustrates reference signals, time-DFS spectra and AoAs of the corresponding scenarios.

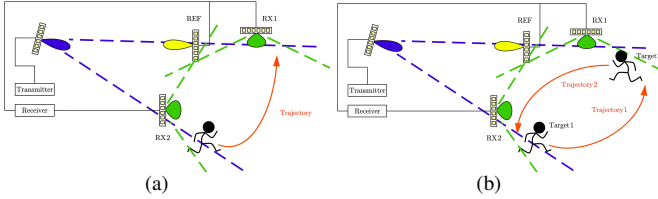


Fig. 5. (a) and (b) are single target and two targets, respectively. The red line is the movement trajectories of experimenters.

REF signals shown in Fig. 6(a) and Fig. 6(b), indicate a fine frame structure to use for communication, even when not aligned with the main lobe at the TX. As for Fig. 6(c) and Fig. 6(e), time-DFS spectra clearly show movement state change of single target, where there exists only one DFS variation curve in each figure, and as for Fig. 6(d) and Fig. 6(f), there exist two main DFS variation curves, representing the respective motions of two targets. A remarkable point is when the first target blocks the transmitted signal, DFS of another target will attenuate even disappear, limited by the poor penetration ability of mmWave, and note that the presence of residual zero-DFS signals in the time-DFS spectra of both scenes since we use Multi-CIT clutter cancellation.

For AoA estimation, each phased array requires 16 beam switches since there have 16 antenna units in mmWave phased arrays. When switching beam pattern, it is assumed that the target does not move since this process can be accomplished in less than 0.5 s (each switch is finished in a few tens of ms). AoA estimation results shown in Fig. 6, where Fig. 6(g) and Fig. 6(i) describe single target scenario and Fig. 6(h) and Fig. 6(j) describe two targets scenario, equal to  $27^\circ, 61^\circ, [-58^\circ, 26^\circ]$ , and  $[-28^\circ, 59^\circ]$ , respectively, corresponding to the ground truth of  $25^\circ, 65^\circ, [-65^\circ, 25^\circ]$ , and  $[-25^\circ, 65^\circ]$ , respectively. For both scenarios, error is limited in  $10^\circ$ , showing the robustness of our system. Discussion further, AoA estimation results of RX1 and RX2 give four intersections, but by increasing receiver phased arrays or excluding intersections that are not in the detection area, the exact starting position of two targets can be derived.

CFAR and clustering results of time-DFS spectrum Fig. 6(f) are shown in Fig. 6(k) and Fig. 6(l), where the number of original clustering categories is 6. Then refine results with estimated AoAs, merge 6 categories into 2 groups (Labels 1, 4, 5 and 6 are merged into one group, labels 2 and 3 are merged into the other group, label -1 is lost as outlier) and use path matching algorithm later. In sake of matching the DFS to each

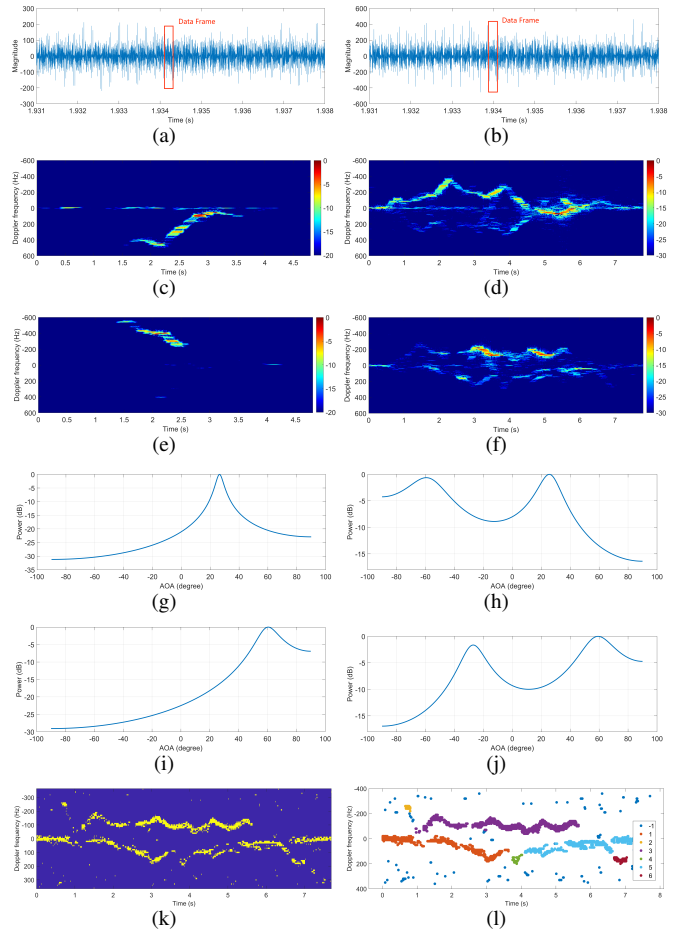


Fig. 6. (a), (c), (e), (g) and (h) obtained from single target scenario show the REF signal, time-DFS spectrum of RX1, time-DFS spectrum of RX2, AoA of RX1 and AoA of RX2, respectively. (b), (d), (f), (h), (j) obtained from two targets scenario have the same meaning as single target results. (k) and (l) is the CFAR and clustering results of (f), respectively.

target, here a trick is proposed. Because the target is assumed to move within range, then the sign and strength of DFS will be referenced when initial position is measured. For instance, when the target is ahead of a phased array, related initial DFS should be negative (away from antennas), otherwise it will leave the detection area. Moreover, when targets bear the same DFS sign, DFS intensity can evaluate the path length to further find the matching target.

### C. Trajectory Reconstruction

Trajectory reconstruction is evaluated in experimental scenarios of single target and multiple targets, where six scenarios are considered. To demonstrate the robustness, each type of movement is tested 20 times performed by various volunteers. Noticed that this section only show the examples.

Three scenarios of single target including straight ahead, turning and circling are shown in Fig. 7. Fig. 7(d) depicts the cumulative distribution functions (CDFs) of tracking error. Observed that for straight ahead, turning and circling, their respective median tracking errors are 10 cm, 11 cm and 7.5 cm, and respective 80<sup>th</sup> percentile errors are 12.7 cm, 15 cm

and 21.2 cm. In the evaluation, it clearly shows that our system effectively captures the trajectory of single target. Note that as the trajectory becomes complex, the error increases as well, especially in the moments when the direction of motion varies, due to the micro Doppler effect of target is excessively strong during the turning, interfering with DFS extraction.

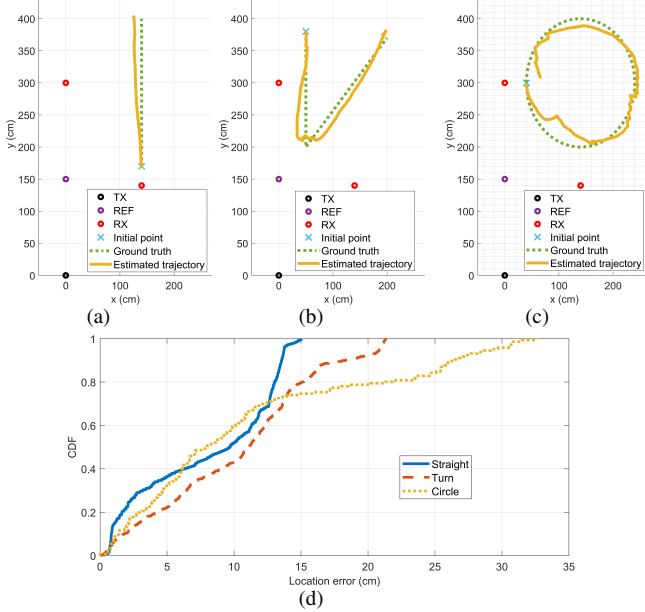


Fig. 7. (a), (b) and (c) describe straight ahead, turning and circling scenarios, respectively. (d) is cumulative distribution function (CDF) of location error.

Fig. 8 illustrates experiments for multiple targets, where three motions are considered including cross walk, relative walk and parallel walk. Fig. 8 (d) shows the CDFs of tracking error, evaluated as the simultaneous error sum of two targets, different from the single target. It can be seen that respective median tracking errors are 19 cm, 18.5 cm, and 20 cm. As illustrated, 80<sup>th</sup> percentile error is within 50 cm for all three type of motions. Noticed that in parallel walk, to avoid identical Doppler features at the same time for two targets, we allow them to move at different velocities. Moreover, compare the scenarios of two targets with those of one target, one more factor for tracking error is that one target blocks the other during the movement. As illustrated in Fig. 8(a), in the first half of the cross walk, the target from below blocks part of the signal, thus the trajectory of the target above appears to be inaccurate and has a larger error, which is a limitation of our system and will be the direction of future improvement.

## VI. CONCLUSION

In this letter, indoor human trajectory reconstruction is realized based on a system of integration of communication and sensing. Specifically, using multiple mmWave phased arrays to transmit and receive multi-carrier signal in 802.11a format while extracting multi-link DFS for velocity estimation and multi-link AoA for initial position estimation, the trajectory of single target or multiple target is recovered accurately. Our system achieves that the median error of single target is lower

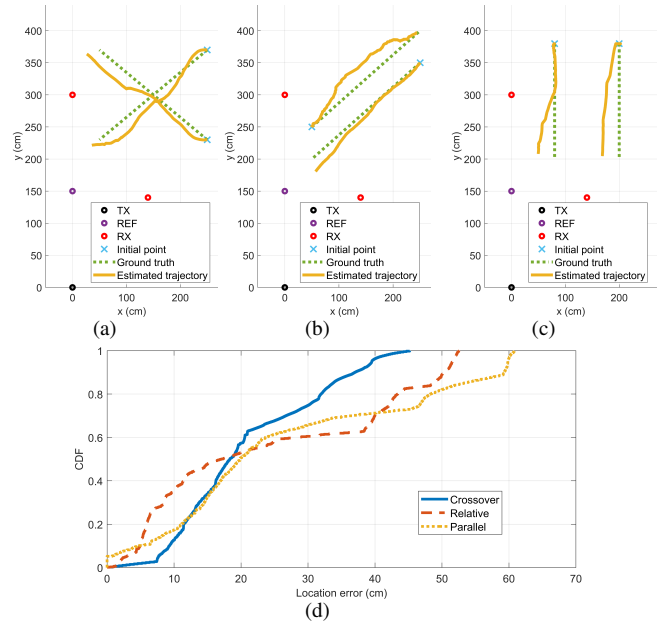


Fig. 8. (a), (b) and (c) describe cross walk, relative walk and parallel walk scenarios, respectively. (d) is the CDF curves of location error.

than 15 cm and two targets is lower than 22 cm. In the future, we will solve the difficulty of object blocking track recovery.

## REFERENCES

- [1] Y. Niu, Y. Li, D. Jin, L. Su, and A. V. Vasilakos, "A survey of millimeter wave communications (mmwave) for 5g: opportunities and challenges," *Wireless Networks*, vol. 21, pp. 2657–2676, 2015.
- [2] K. Qian, C. Wu, Z. Yang, Y. Liu, and K. Jamieson, "Widar: Decimeter-level passive tracking via velocity monitoring with commodity wi-fi," in *Proceedings of the 18th ACM International Symposium on Mobile Ad Hoc Networking and Computing*, 2017, pp. 1–10.
- [3] X. Li, S. Li, D. Zhang, J. Xiong, Y. Wang, and H. Mei, "Dynamic-MUSIC: Accurate device-free indoor localization," in *Proceedings of the 2016 ACM International Joint Conference on Pervasive and Ubiquitous Computing*, 2016, p. 196–207.
- [4] K. Qian, C. Wu, Y. Zhang, G. Zhang, Z. Yang, and Y. Liu, "Widard 2.0: Passive human tracking with a single wi-fi link," in *Proceedings of the 16th Annual International Conference on Mobile Systems, Applications, and Services*, 2018, pp. 350–361.
- [5] K. Niu, X. Wang, F. Zhang, R. Zheng, Z. Yao, and D. Zhang, "Rethinking doppler effect for accurate velocity estimation with commodity wifi devices," *IEEE Journal on Selected Areas in Communications*, vol. 40, no. 7, pp. 2164–2178, 2022.
- [6] C. Wu, F. Zhang, B. Wang, and K. R. Liu, "mmtrack: Passive multi-person localization using commodity millimeter wave radio," in *IEEE INFOCOM 2020-IEEE Conference on Computer Communications*, 2020, pp. 2400–2409.
- [7] R. Zhou, M. Tang, Z. Gong, and M. Hao, "Freetrack: Device-free human tracking with deep neural networks and particle filtering," *IEEE Systems Journal*, vol. 14, no. 2, pp. 2990–3000, 2019.
- [8] D. K. Tan, H. Sun, Y. Lu, M. Lesturgie, and H. L. Chan, "Passive radar using global system for mobile communication signal: theory, implementation and measurements," *IEE Proceedings-Radar, Sonar and Navigation*, vol. 152, no. 3, pp. 116–123, 2005.
- [9] W. Li, R. J. Piechocki, K. Woodbridge, C. Tang, and K. Chetty, "Passive wifi radar for human sensing using a stand-alone access point," *IEEE Transactions on Geoscience and Remote Sensing*, vol. 59, no. 3, pp. 1986–1998, 2020.
- [10] A. Hinneburg, "A density based algorithm for discovering clusters in large spatial databases with noise," in *KDD Conference*, 1996, 1996.
- [11] Y. Sun, J. Li, T. Zhang, R. Wang, X. Peng, X. Han, and H. Tan, "An indoor environment sensing and localization system via mmwave phased array," *Journal of Communications and Information Networks*, vol. 7, no. 4, pp. 383–393, 2022.